Leukemia (2016) **30,** 1103–1115

www.nature.com/leu

ORIGINAL ARTICLE

Targeting vasculogenesis to prevent progression in multiple myeloma

M Moschetta[1,2], Y Mishima[1], Y Kawano[1], S Manier[1], B Paiva[3], L Palomera[4], Y Aljawai[1], A Calcinotto[5], C Unitt[6], I Sahin[1], A Sacco[1], S Glavey[1], J Shi[7], MR Reagan[1,8], F Prosper[3], M Bellone[5], M Chesi[9], LP Bergsagel[9], A Vacca[2], AM Roccaro[1,10] and IM Ghobrial[1]

The role of endothelial progenitor cell (EPC)-mediated vasculogenesis in hematological malignancies is not well explored. Here, we showed that EPCs are mobilized from the bone marrow (BM) to the peripheral blood at early stages of multiple myeloma (MM); and recruited to MM cell-colonized BM niches. Using EPC-defective ID1+/− ID3 −/− mice, we found that MM tumor progression is dependent on EPC trafficking. By performing RNA-sequencing studies, we confirmed that endothelial cells can enhance proliferation and favor cell-cycle progression only in MM clones that are smoldering-like and have dependency on endothelial cells for tumor growth. We further confirmed that angiogenic dependency occurs early and not late during tumor progression in MM. By using a VEGFR2 antibody with anti-vasculogenic activity, we demonstrated that early targeting of EPCs delays tumor progression, while using the same agent at late stages of tumor progression is ineffective. Thus, although there is significant angiogenesis in myeloma, the dependency of the tumor cells on EPCs and vasculogenesis may actually precede this step. Manipulating vasculogenesis at an early stage of disease may be examined in clinical trials in patients with smoldering MM, and other hematological malignancies with precursor conditions.

Leukemia (2016) **30,** 1103–1115; doi:10.1038/leu.2016.3

INTRODUCTION

Increased angiogenesis is associated with progression of hematological malignancies,[1,2] and correlates with shorter overall survival and resistance to therapy.[3] These observations led to the assumption that anti-angiogenic agents would be effective in multiple myeloma (MM), as they are for several types of solid tumors.[4] However, selective anti-angiogenic drugs have not shown promise therapeutic activity as single agents in clinical trials for hematological malignancies,[5] specifically for MM.[6]

Most studies have focused on neoangiogenesis as the principal mechanism that drives MM-associated vessel formation in the BM,[7] but other mechanisms possibly contributing to this process[8] (that is, vascular co-option, vasculogenic mimicry and endothelial progenitor cell (EPC)-mediated post-natal vasculogenesis) remain ill defined.

EPCs are BM-derived circulating precursors that can home to the tumor bed, secrete pro-angiogenic growth factors and differentiate into endothelial lineage cells through a process known as 'post-natal vasculogenesis', thereby contributing to vessel formation.[9] The role of EPCs in regulating tumor progression in cancers (such as MM) that already reside in the BM has not been studied.[9] Here, we explore the functional role of EPC trafficking in a hematological malignancy such as MM, and test the hypothesis that targeting these cells at the early stages of the 'angiogenic switch',[10] before the occurrence of active progression, can halt disease progression.

MATERIALS AND METHODS

Cells

MM cell lines (human MM1.S, MM1.S-GFP-luc+, MM1.S-RFP-luc+ and IM9, and murine 5TGM1 and Vk12598 cells) and human umbilical vein endothelial cells (HUVECs) were used in this study as described in Supplementary Methods. MM patient samples were obtained after approval from the Dana-Farber Cancer Institute Institutional Review Board (DFCI IRB). Informed consent was obtained from all patients in accordance with the Declaration of Helsinki. Peripheral blood (PB) mononuclear cells (PBMCs) were isolated as detailed in Supplementary Methods.

Detection of EPCs in the PB of patients with MM

PBMCs were isolated from PB of MM patients at different stages of disease,[11] and processed as described in Supplementary Methods.

In vitro endothelial cell - colony forming unit (EC-CFU) and endothelial colony forming cells (ECFC) colony-forming assays

A 15-ml sample of venous blood was used for the EC-CFU or ECFC colony assays. EC-CFU and ECFC colony assays were performed as previously described[12,13] with some modifications, and as detailed in Supplementary Methods.

MM cell proliferation assay and MM cell sorting in the co-culture system

MM1.S-GFP-luc+ and MM1.S-RFP-luc+ cells were plated at 1×10^4 cells/well in a BD Falcon 96-well plate (BD Falcon, Bedford, MA, USA), alone or in co-culture with HUVECs (3×10^3 cells) or primary ECFCs (3×10^3). Detailed description of co-culture experiments is provided in Supplementary Methods.

[1]Medical Oncology, Harvard Medical School, Dana-Farber Cancer Institute, Boston, MA, USA; [2]University of Bari Medical School, Bari, Italy; [3]Clinica Universidad de Navarra, Centro de Investigaciones Medicas Aplicadas (CIMA), Pamplona, Spain; [4]Hospital Clinico Universitario Lozano Blesa, Zaragoza. Spain; [5]Cellular Immunology Unit, IRCCS San Raffaele Scientific Institute, Milano, Italy; [6]Dana Farber/Harvard Cancer Center, Boston, MA, USA; [7]Department of Biostatistics, Harvard School of Public Health, Boston, MA, USA; [8]Maine Medical Center Research Institute, Scarborough, ME, USA; [9]Comprehensive Cancer Center, Mayo Clinic, Scottsdale, AZ, USA and [10]Spedali Civili di Brescia, Centro Ricerca Ematooncologica AIL (CREA), Department of Hematology, Brescia, Italy. Correspondence: Dr AM Roccaro or Dr IM Ghobrial, Medical Oncology, Dana-Farber Cancer Institute, 450 Brookline Avenue, Boston, MA 02115, USA.
Email: aldo_roccaro@dfci.harvard.edu or irene_ghobrial@dfci.harvard.edu
Received 7 August 2015; revised 9 November 2015; accepted 16 December 2015; accepted article preview online 3 February 2016; advance online publication, 11 March 2016

Tube formation assay

HUVECs (2.5×10^4 per well) or cells derived from ECFC colonies (ECFCs) (2.5×10^4 per well) were seeded on growth factor reduced Matrigel (BD Biosciences, San Jose, CA, USA) pre-coated 96-well plate, and in colony medium for 16 h, and tube formation was assessed by light microscopy as previously described.[14]

Live confocal microscopy

Five $\times 10^5$ HUVECs or ECFCs were seeded in 12-well glass bottom plate (MatTek, Ashland, MA, USA) and cultured in colony medium. Staining procedures and imaging acquisition are described in Supplementary Methods.

MM1.S-GFP-luc+ and MM1.S RFP-luc+ xenografts and *in vivo* anti-VEGFR2 therapy with DC101

MM1.S-GFP-luc+ and MM1.S-RFP-luc+ xenografts were generated as described in Supplementary Methods. DC101 anti-murine VEGFR2 Ab (Eli Lilly & Co., Indianapolis, IN, USA) therapeutic activity was evaluated *in vivo* in the MM1.S-GFP-luc+ orthotopic xenograft model as described in Supplementary Methods and as previously reported.[15]

Transgenic mice experiments

ID3 −/− mice and ID1 −/− mice in a mixed C57Bl6/129Sv background were kindly provided by Dr Benezra R (Memorial Sloan–Kettering Institute, NY, USA). Mice were backcrossed onto C57BL/6 background (Jackson Laboratories, Ban Harbor, ME, USA) for 4–5 generation, and then crossed to obtain ID1+/+ ID3+/+ mice (wild-type littermates) and ID1+/− ID3 −/− mice. Genotyping was performed by using Transnetyx automated genotype service (Transnetyx Inc., Cordova, TN, USA). Details of experiments involving ID1+/− ID3 −/− mice are provided in Supplementary Methods.

Serum electrophoresis, serum total and gamma protein quantification

Serum electrophoresis, serum total and gamma protein quantification have been performed as previously described and as detailed in Supplementary Methods.[16]

Detection of EPCs in the PB of transgenic Vk*MYC mice

Transgenic Vk*MYC mice with early MM disease (early MM t-Vk*MYC, $n = 12$), late MM disease (late MM t-Vk*MYC, $n = 9$) according to the M-spike quantification by electrophoresis of the serum protein (SPEP) (6% M-spike area under curve of the SPEP pattern was used as cutoff) and healthy C57BL/6 mice ($n = 11$) were bled at retro-orbital site.

After, the PB was lysed to obtain PBMCs; these were then washed with PBS and FcR blocker (BD Biosciences), and stained with eFluor450-anti-mouse CD34 (eBiosciences, San Diego, CA, USA, clone: RAM34), and Alexa Fluor 647-anti-mouse VEGFR2 (BioLegend, San Diego, CA, USA, clone: 89B3A5) antibodies for 30 min on ice, and acquired on a BD LSR Fortessa flow-cytometry system (BD Biosciences). Data were analyzed using the FlowJo software (TreeStar Inc., Ashland, OR, USA).

SCID-mu model characterization and recruitment model

Full methods of SCID-mu and recruitment model characterization are provided in Supplementary Methods.

Bone marrow transplantation studies

Six- to eight-week-old healthy SCID-bg mice were lethally irradiated (450 rads) and injected with $4–5 \times 10^6$ BM cells collected from SCID-GFP mice. After 4–5 weeks, engraftment was confirmed by flow-cytometry study of GFP+ cells on PBMCs from transplanted mice.

Wild-type littermate mice and ID1+/− ID3 −/− mice were lethally irradiated (950 rads) at 8 weeks of age. Approximately 4×10^6 wild-type bone marrow (BM) cells isolated from wild-type littermates were injected intravenously (i.v.) into tail veins of irradiated recipient mouse. Mice were used for experiments 4–5 weeks after BM transplantation.

Histological analysis and CD34 BM microvessel density quantification

Histological analysis and CD34 BM microvessel density (MVD) quantification have been performed as reported,[10,17] and as detailed in Supplementary Methods.

PB and BM EPC quantification and proliferation by cytometry by time-of-flight

PB was obtained by sub-mandibular bleeding, and processed as described above for PBMC isolation. BM cells were obtained at the time of killing the mice through flushing of femurs with 1× PBS, as previously described.[17] cytometry by time-of-flight studies were performed as previously reported.[18,19] A detailed description of the Methods is reported in Supplementary Data.

Clear, unobstructed brain/body imaging cocktails and computational analysis-femur preparation and *ex vivo* BM confocal microscopy

To observe the intra-bone tumor cells and functional vessels, we performed confocal-microscopic observation of femurs that were treated with the recently developed transparent technology.[20] Details are provided in Supplementary Methods.

Library construction, RNA-sequencing and RNA-sequencing data analysis

Full description is provided in Supplementary Methods.

Statistical analysis

Statistical analysis was performed with GraphPad Prism Software (Prism, GraphPad Software Inc., La Jolla, CA, USA). The unpaired Student's *t*-test was used to compare two independent groups for continuous end points if normally distributed. One-way ANOVA was used when three or more independent groups were compared. For survival data, Kaplan–Meier curves were plotted and compared using a log-rank test. All tests were two-sided. A P-value of less than 0.05 was considered as statistically significant.

RESULTS

MM patients present with increased levels of circulating EPCs

We used flow cytometry to assess the numbers of circulating EPCs (CD34+VEGFR2+ cells)[21] in the PB of MM patients at different stages of disease, including monoclonal gammopathy of uncertain significance (MGUS) patients, smoldering MM (sMM) and active MM (MM) diagnosed according to the 2009 International Myeloma Working Group criteria.[11] Similar studies were also performed in and healthy donors as a control. The EPC gating strategy is shown in Supplementary Figure 1A. CD34+ VEGFR2+ EPC levels were significantly increased (7- to 10-fold, $P < 0.005$) in sMM and MM patients compared with healthy individuals (Figure 1a), indicating that EPC circulation occurs at early stages of progression, even at the smoldering stage, before active disease progression occurs. We did not observe significant differences in levels of circulating EPCs between MGUS patients and healthy donors (Figure 1a).

We next performed quantification of EPCs in the PB of MM patients, and healthy controls with the use of two *in vitro* colony-forming assays: the endothelial colony-forming cell (late outgrowth EPCs, ECFC assay) and the endothelial cell (EC) colony-forming unit (early outgrowth EPCs, EC-CFU assay) assays.[9] The ECFC assay allows quantification of the putative hemangioblast-derived EPC population.[22,23] ECFC colonies were indeed characterized by a high proliferative activity and the cobblestone morphology typical of ECs (Figure 1b). Cells from these colonies formed capillary-like tubes when seeded on matrigel, in a similar manner to HUVECs that were used as a control (Figure 1b). The ECFC phenotype was examined with live confocal microscopy; the cells showed positive expression of EC-specific markers, including CD34, CD31 and VE-Cadherin (Figure 1c), but lacked CD45 expression (Supplementary Figure 1B). Flow-cytometry analysis further confirmed that ECFCs were positive for CD34, CD31, VE-Cadherin, VEGFR2 and Tie2/Tek, but negative for CD45 and CD133 expression, thus recapitulating the conventional phenotype of HUVECs (Supplementary Figure 2A). Together, these

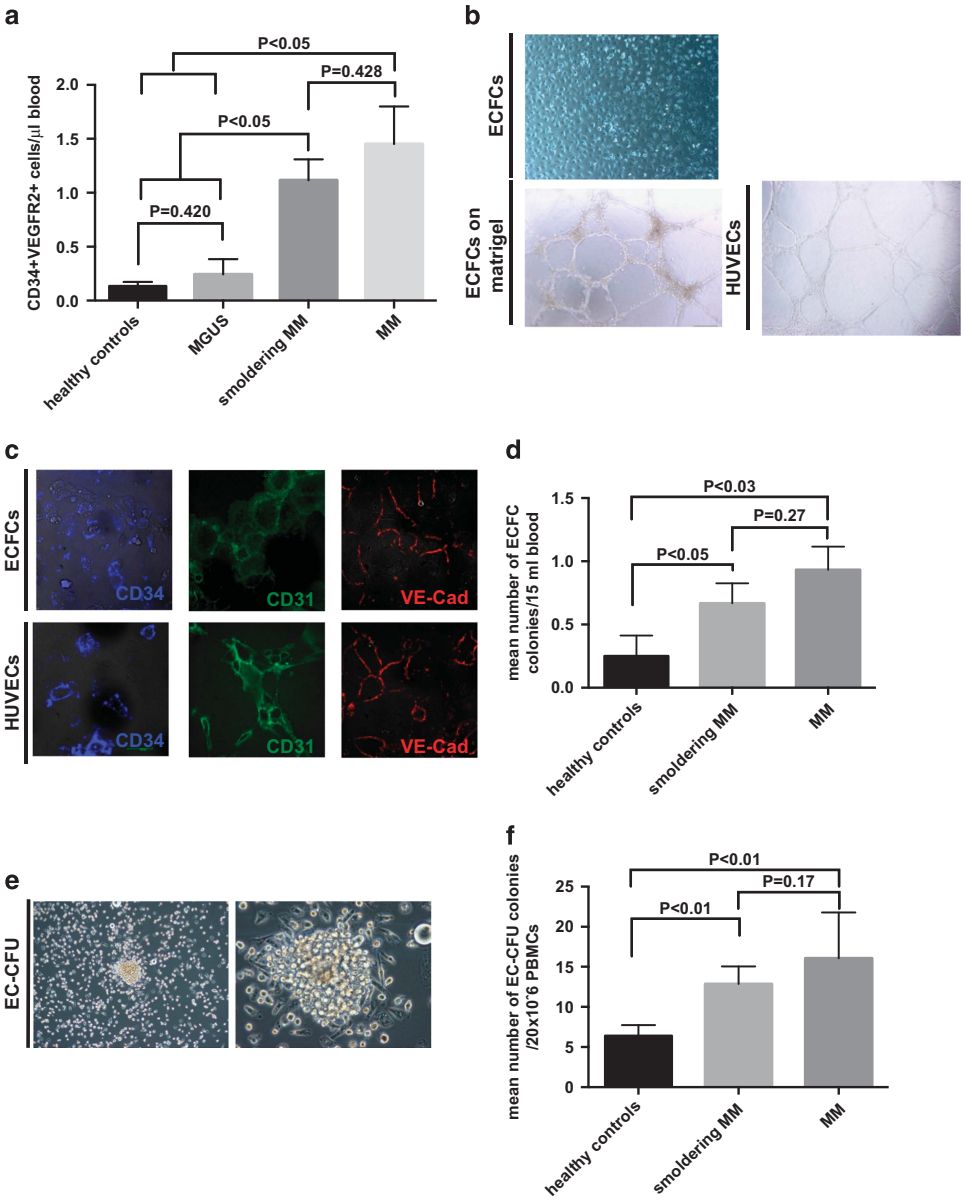

Figure 1. Circulating EPC levels are increased in MM patients. (**a**) Circulating CD34+VEGFR2+ cell (EPCs) levels were quantified by flow cytometry in PB of healthy donor controls ($n=11$), MGUS patients ($n=5$), sMM patients ($n=12$) and active MM patients (MM, $n=19$). Presence of EPCs was expressed as EPCs/µl. MM patients but not MGUS patients presented with a significant increase in EPCs compared with healthy donor controls. (**b**) ECFC colony presented cobblestone morphology typical of mature ECs (upper panel, ×10 magnification), and are able to form capillary-like structures when seeded on matrigel (middle panel, ×10 magnification) similarly to HUVEC cells (lower panel, ×10 magnification). (**c**) CD34, CD31 and VE-cadherin expression by live confocal microscopy (×63.5 magnification) in cells from an ECFC colony (ECFCs, left panels) and in HUVECs (right panels). (**d**) Mean ECFC colony number per 15 ml PB obtained from PBMCs of healthy donor controls ($n=5$), sMM patients ($n=8$), MM patients ($n=14$). Smoldering and MM patient PBMCs presented a significantly higher colony-forming ability compared with healthy donor controls. Data expressed as mean+s.e.m. *P* indicates *P*-value. (**e**) Representative EC-CFU colony (×10 magnification upper left panel, ×20 magnification upper right panel). (**f**) Mean EC-CFU colonies obtained from PBMCs from healthy donor controls ($n=8$), sMM patients ($n=15$), MM patients ($n=15$) per 20×10^6 PBMCs. Data expressed as mean+s.e.m. *P* indicates *P*-value.

results indicate that ECFC colonies are formed by mature ECs that are derived by trans-differentiation of hemangioblast-derived circulating EPCs. Importantly, the ECFC colony-forming ability of PBMCs from both sMM and MM patients was significantly higher compared with that of control donor PBMCs (Figure 1d, 0.93 and 0.66 ECFC colonies/15 ml of blood for MM and sMM, respectively, versus 0.25 ECFC colonies/15 ml of blood for control donors, $P<0.05$).

The early outgrowth EPCs, which include other circulating precursor cells of hematopoietic origin with vasculogenic ability,[23,24] were quantified with use of the EC-CFU colony-forming assay. Figure 1e shows a representative EC-CFU colony that appeared 10–15 days after culturing PBMCs on fibronectin and in EC-specific growth medium: in contrast to the ECFC colonies, EC-CFU colonies disappeared after a more prolonged time in culture, as reported.[23,24]

PBMCs from the PB of sMM and MM patients displayed a significantly higher EC-CFU colony-forming ability compared with those from the PB of donor controls (Figure 1f, all $P<0.01$ compared with controls); PBMCs from patients with active MM showed the highest EC-CFU colony-forming ability (16 EC-CFU

colonies/20×10^6 PBMCs for MM versus 6.4 EC-CFU colonies/20×10^6 for controls). In line with the previous reports,[23] flow-cytometry studies showed that cells from these colonies expressed EC-specific markers (CD34, CD31 and VEGFR2) and also CD45, confirming their hematopoietic origin (Supplementary Figure 2B).

Collectively, these results indicate that levels of circulating EPCs are increased in MM patients,[25,26] and show that sMM patients present with enhanced vasculogenic activity and higher levels of EPCs, suggesting that the process of vasculogenesis occurs early during MM progression.

Evaluation of circulating EPC levels and EPC proliferation using murine MM mouse models

To further confirm that EPCs increase in number and trafficking in early stages of smoldering-llke MM, we measured levels of circulating CD34+VEGFR2+ EPCs[27,28] in the PB of Vk*MYC transgenic mice[29] at different stages of disease development, as recently reported.[30] These included early (smoldering-like) stages (M-spike lower than 6% area under curve of the SPEP, early t-MM Vk*MYC) to stages of overt MM (M-spike higher than 6% area under curve of the SPEP, late t-MM Vk*MYC) (Figure 2a), and compared them with levels in PB of control C57BL/6 wild-type mice.

Levels of circulating EPCs were significantly higher in both early t-MM Vk*MYC and late t-MM Vk*MYC, compared with wild-type mice (7.5 times and 4.5 times higher, respectively, compared with healthy control mice; $P < 0.05$), indicating that EPC circulation occurs at early stages of disease progression, and confirming our observation on patient samples (Figures 2b and c). No significant differences in EPC levels were observed between the early t-MM Vk*MYC and late t-MM Vk*MYC mouse groups (Figure 2b).

The Vk*MYC-derived transplantable Vk12598 model has recently been reported to be a reliable murine MM model,[16] and it is the only transplantable MM model that can be used in a C57BL/6 background[31] thus allowing studies in genetic modified mouse models. We first injected a group of mice with Vk*MYC cells, and killed them at an early (±2 weeks after tumor cell injection) and a late (±4 weeks after tumor cell injection) time point. The transplantable MM cells presented with a progressive accumulation of CD138+ cells in the BM, and the typical appearance of the M-spike by SPEP recapitulating features of MM progression (Supplementary Figure 3A). Also, mice with early and late Vk*MYC MM disease presented with a 3.1- and 4.4-fold enhancement in BM MVD, respectively, compared with healthy C57BL/6 mice (Supplementary Figure 3B). These results show that progression of Vk12598 MM disease in the BM is indeed

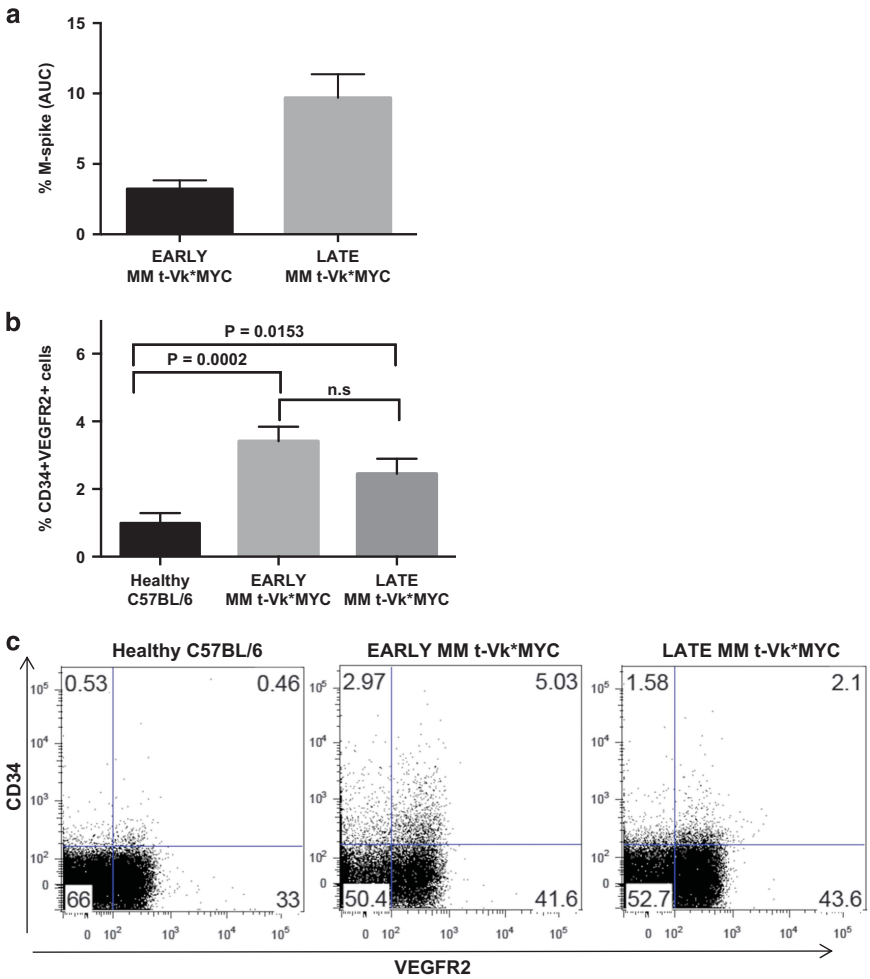

Figure 2. Circulating EPCs increase early during progression of MM in murine models. (**a**) M-spike quantification in early ($n = 12$) and late ($n = 9$) transgenic MM Vk*MYC mice (MM t-Vk*MYC) express as percentage of area under curve (% M-spike AUC) of a serum electrophoresis (SPEP) pattern. 6% M-spike AUC of SPEP has been used as a cutoff to distinguish early and late MM t-Vk*MYC. (**b**) Circulating CD34+VEGFR2+ cell levels were evaluated in PB of healthy C57BL/6 mice ($n = 11$), early MM t-Vk*MYC ($n = 12$) and late MM t-Vk*MYC ($n = 9$) mice using flow cytometry. *P* indicates *P*-values. (**c**) Representative CD34/VEGFR2 dot plots from a healthy C57BL/6 mice, an early MM t-Vk*MYC and a late MM t-Vk*MYC showing an increase in circulating CD34+ VEGFR2+ EPCs in MM bearing mice.

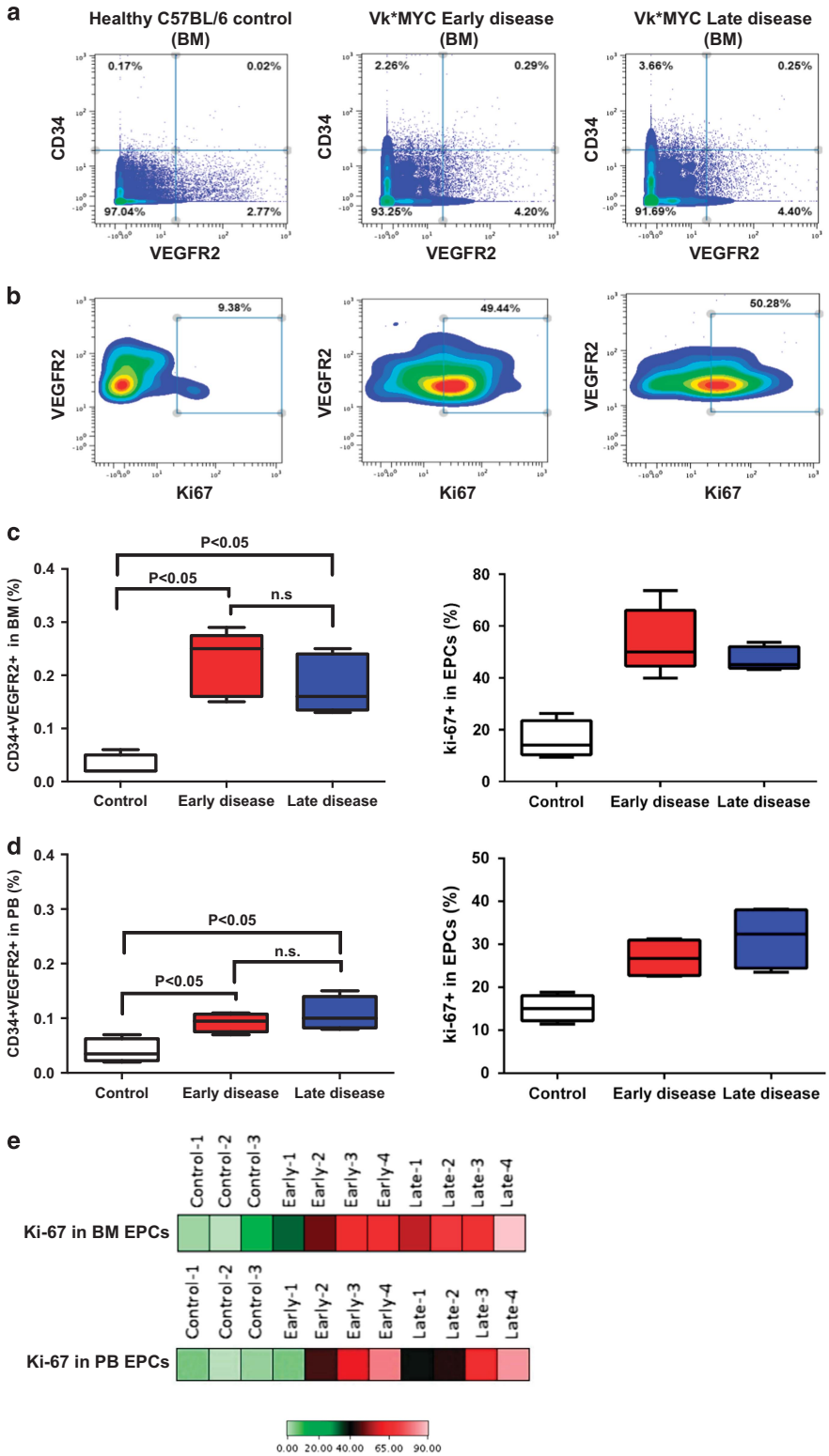

Figure 3. Transplantable Vk*MYC model progression is accompanied by increased levels and proliferation of EPCs in both PB and BM. (**a**) Representative CD34/VEGFR2 dot plots of BM EPCs (CD34+VEGFR2+ cells) of a healthy C57BL/6 mouse (left panel), a Vk*MYC cell injected mouse with early MM disease (±15–18 days after tumor cell injection, middle panel) and a VK*MYC cell injected mouse with late MM disease (±28–35 days after tumor cell injection, right panel) studied by cytometry by time-of-flight and analyzed by Cytobank software. (**b**) Ki-67 expression in gated EPCs (CD34+VEGFR2+) of the same mice showing proliferation of BM EPCs in tumor-bearing mice (middle and right panels) but not in naive mice (left panel). (**c**) Mean percentage (%) of EPCs in BM of healthy C57BL/6 mice ($n=3$), VK*MYC cell injected mice with early ($n=4$) and late ($n=4$) MM disease (left graph), and mean Ki-67 expression (%) in BM EPCs of the same mice (right graph). (**d**) Mean % of EPCs in PB of healthy C57BL/6 mice ($n=3$), VK*MYC cell injected mice with early ($n=4$) and late ($n=4$) MM disease (left graph), and mean Ki-67 expression (%) in PB EPCs of the same mice (right graph). (**e**) Heatmap analysis of Ki-67 expression (%) in BM (upper lane) and PB (lower lane) EPCs of healthy C57BL/6 mouse, Vk*MYC cell injected mice with early and late MM disease. Graph bar indicates % of Ki-67 positivity in PB and BM EPCs of single mouse studied. Values express as mean % ± s.e.m. *P* indicates *P*-value.

accompanied by a progressive increase in MVD, similar to that described for MM patients.[32,33] In the same groups of mice, we also used cytometry by time-of-flight to study EPC levels and the rate of EPC proliferation, in BM (Figures 3a and c) and in PB (Figure 3d); we found that EPC levels were significantly increased, compared with healthy mice, in early as well as late stage of the disease; no significant differences in EPC levels were observed between the early and late groups of mice. Notably, Ki-67 co-staining of EPCs in BM and PB showed that an enhanced proliferation rate of EPC in tumor-bearing mice at early and late disease stages relative to that of healthy C57BL/6 mice (Figures 3c–e). These findings suggest that in the Vk12598 transplantable model, EPCs are mobilized, and proliferate in both the PB and the BM, even in early (smoldering-like) stages of MM disease progression.

EPCs are recruited to areas of tumor growth within MM BM niches

To study whether EPCs can be mobilized from one area of the BM, and recruited to a different BM site where malignant cells are growing, we generated a new mouse model, referred as the SCID-mu model: in this model, syngenic femurs were implanted subcutaneously into recipient SCID-bg mice previously transplanted with BM from SCID-GFP mice, such that trafficking of host BM-derived cells (GFP+ cells) from one site of the BM to another

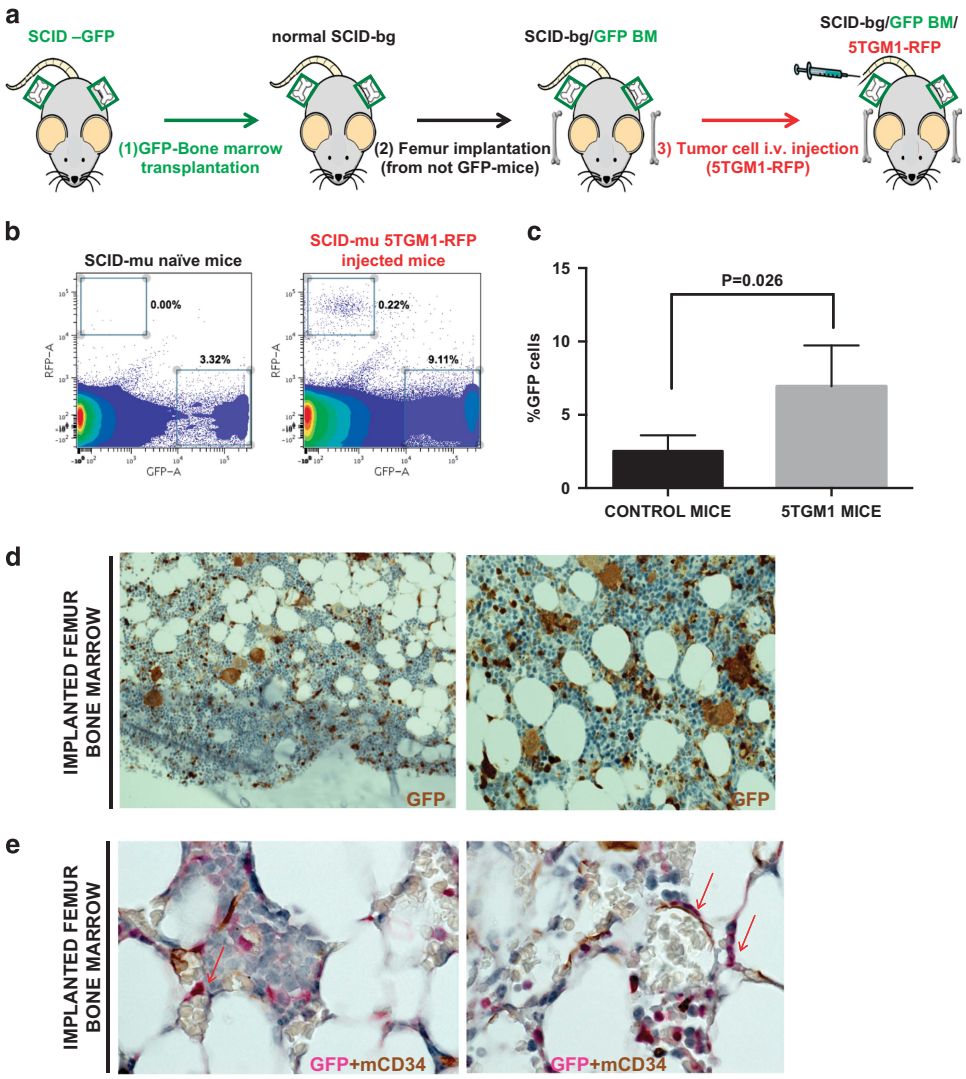

Figure 4. SCID-mu recruitment model**.** (**a**) Schematic representation of the experimental procedure of the SCID-mu recruitment model. SCID-bg mice are transplanted with BM from SCID-GFP mice (1); after GFP-BM transplantation, these mice are implanted with femurs from SCID-bg mice (2), and i.v. injected with MM-RFP+ cells 2 weeks after femur implantation (two femur each mouse) (3). In this model, host BM cells are GFP+, while the BM cells resident in the implanted femur are GFP − . (**b**) Flow-cytometry study of flushed BM cells from implanted femurs of tumor cell injected versus not injected mice. Panels are representative dot-plot panels showing RFP+ and GFP+ cells in the BM flushed cells of an implanted femur from a naive mouse and a 5TGM1-RFP+ cell i.v injected mouse. Only 5TGM1-RFP+ cell injected mouse present RFP+ MM cells in the implanted femur (right panel); tumor cell injected mice presented an increase in the % of GFP+ cells in the flushed BM (right panel) compared with not injected mice. (**c**) The % of GFP+ cells was significantly higher in flushed BM cells from 5TGM1-RFP injected mice compared with not injected mice, suggesting that MM cells recruit BM-derived cells. *P* indicates *P*-value. (**d**) IHC studies of GFP+ cells (brown) in the implanted femur of a representative 5TGM1-RFP+ cell injected mouse, showing GFP cells of different morphology commingled with BM resident GFP − cells (×20 magnification left panel, × 40 magnification right panel). (**e**) Double CD34 (brown) and GFP (pink) IHC staining of an implanted femur from a representative 5TGM1-RFP injected mouse showing occasional CD34/GFP double-positive cells lining BM vessels containing red blood cells (×100 magnification), indicating that the process of vasculogenesis takes place in the BM.

could be examined (Supplementary data and Supplementary Figure 4). We first engrafted normal SCID-bg mice with SCID-GFP BM cells to track host BM-derived GFP+ cells; following this (Supplementary Figure 5), engrafted mice were implanted with femurs from normal SCID-bg mice, and 2 weeks after implantation, mice were injected (i.v.) with 5TGM1-RFP+ MM murine cells, which home to and engraft in the host as well as implanted femurs (Figure 4a).

When the mice developed paralysis, they were killed, the implanted femurs were harvested and used for flow-cytometry

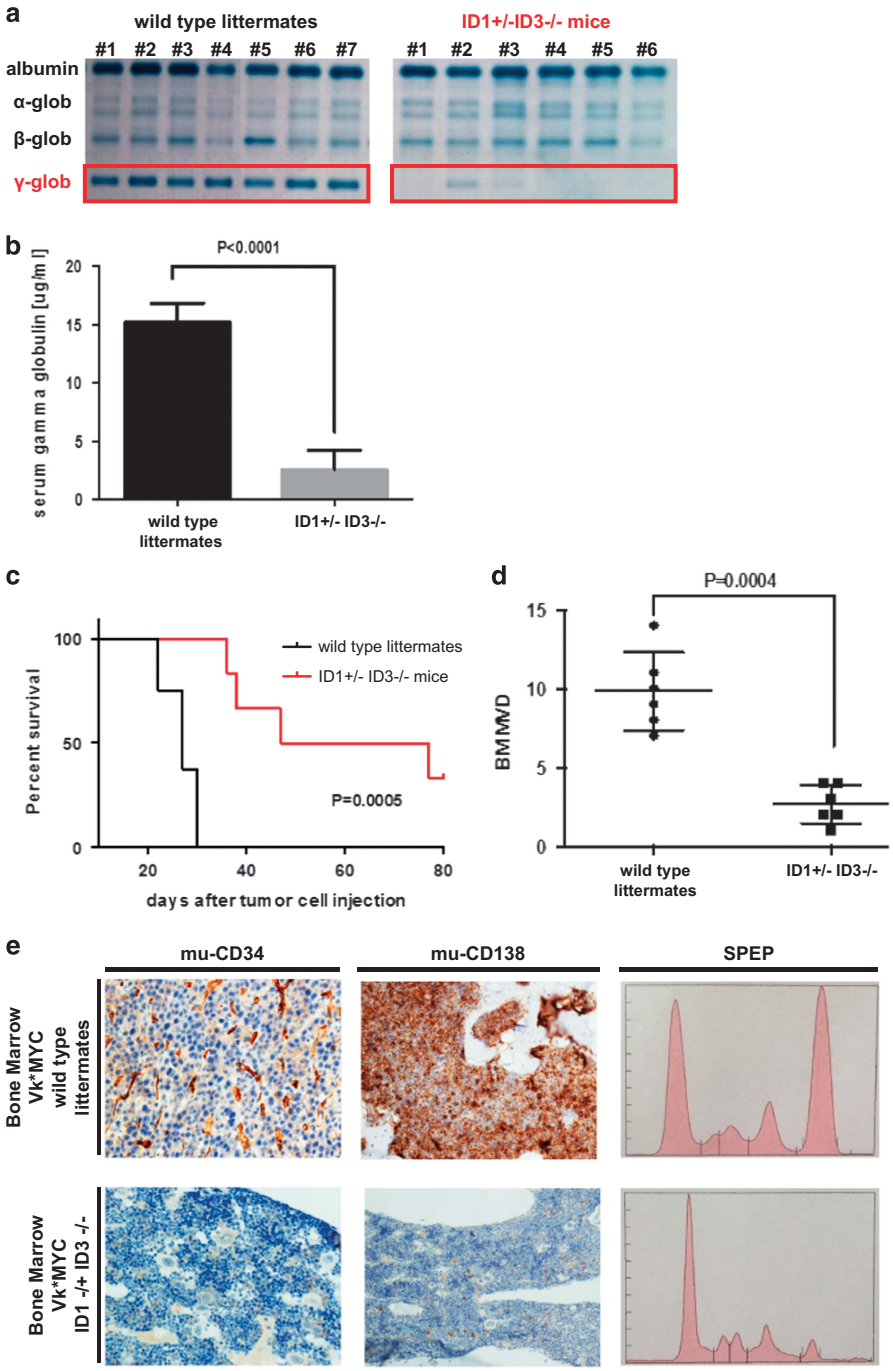

Figure 5. Transplantable Vk*MYC model progression is impaired in EPC-defective ID1+/− ID3−/− transgenic mice. (**a**) SPEP agarose gel results in the group of wild-type littermates (left gel, $n=7$) and ID1+/− ID3−/− mice (right gel, $n=6$) 3 weeks after injection of Vk*MYC transplantable cell line (4×10^6 total spleen cells) showing the presence of an M-protein in the gamma region of the SPEP pattern of higher intensity in the group of wild-type littermates compared with that of ID1+/− ID3−/− mice. (**b**) Serum gamma globulin concentration estimated by QuickScan 2000 software in the same groups of mice and at the same time point. Values expressed as mean+s.e.m. *P* indicates *P*-value. (**c**) Kaplan–Meier survival curves of wild-type littermates ($n=8$), and ID1+/− ID3−/− mice ($n=6$) injected with transplantable Vk*MYC cells (4×10^6 total spleen cells). *P* indicated *P*-value by log-rank test. (**d**) BM MVD quantification performed after CD34 IHC staining on BM slides from Vk*MYC injected wild-type littermates ($n=3$, 2×40 fields per mouse) and ID1+/− ID3−/− mice ($n=3$, 2×40 field per mouse) killed *ad interim* 3 weeks after tumor cell injection. (**e**) CD34 (left panels) and CD138 (middle vertical panels) IHC studies of BM sections from a representative Vk*MYC injected wild-type littermate (upper horizontal panels), and a Vk*MYC cell injected ID1+/− ID3−/− mouse. Right panels show SPEP results of the correspondent mice.

and immunohistochemistry (IHC) studies: the presence of 5TGM1-RFP+ cells was confirmed within the BM of implanted femurs in mice that were injected with tumor cells (Figure 4b); levels of total GFP+ cells were significantly increased (7.92 ± 2.4% versus 2.63 ± 0.89%) in implanted femurs in tumor injected mice compared with control mice (Figure 4c, $P < 0.03$), indicating that BM cells were mobilized from the host BM and recruited to BM areas colonized by malignant cells. GFP-IHC staining of implanted femurs showed that host BM-derived GFP+ cells were commingled with resident non-GFP BM cells (Figure 4d). Importantly, double labeling for GFP and mouse CD34 revealed that GFP+ CD34+ cells were integrated in the BM vessels of implanted femurs (Figure 4e, arrows). These results indicate that the process of vasculogenesis occurs within the BM niche during MM growth and results from recruitment of BM-derived cells from distant BM sites.

EPCs promote MM progression *in vivo*

We then used the ID1+/− ID3−/− mouse model to investigate whether EPCs are involved in MM tumor progression. We chose this model for its specific defect in BM-derived EPCs,[34,35] together with a normal representation of other hematopoietic-derived cell populations[36] including other BM-derived pro-angiogenic hematopoietic cell types (that is, Tie2 expressing monocytes, tumor associated macrophages and neutrophils). This model has been previously extensively characterized.[34,35] We examined the *in vivo* tumor growth of Vk12598 cells transplanted in ID1+/− ID3−/− mice. Parameters of disease development and survival were evaluated after injecting Vk12598 cells in ID1+/− ID1−/− mice and wild-type littermates. A significant decrease in tumor burden was noted in ID1+/− ID3−/− mice injected with Vk12598 cells, relative to control mice, as evidenced by quantifying the M-spike by SPEP (Figures 5a and b). Moreover, survival of ID1+/− ID3−/− tumor engrafted mice was significantly longer compared with wild-type controls, with approximately 1/3 of the ID1+/− ID3−/− mice developing no signs of disease progression for up to 125 days after injection of tumor cells (Figure 5c). BM MVD and numbers of infiltrated BM Vk12598 cells and were significantly lower 3 weeks after tumor cell injection in ID1+/− ID3−/− mice compared with wild-type littermates (Figures 5d and e). Taken together, these results indicate that EPCs are critical for MM progression.

Wild-type BM transplantation restores Vk*MYC tumor growth in ID1+/− ID3−/− transgenic mice

To further confirm that the previous results obtained in ID1+/− ID3−/− mice depend on BM-derived EPC defect of these mice,

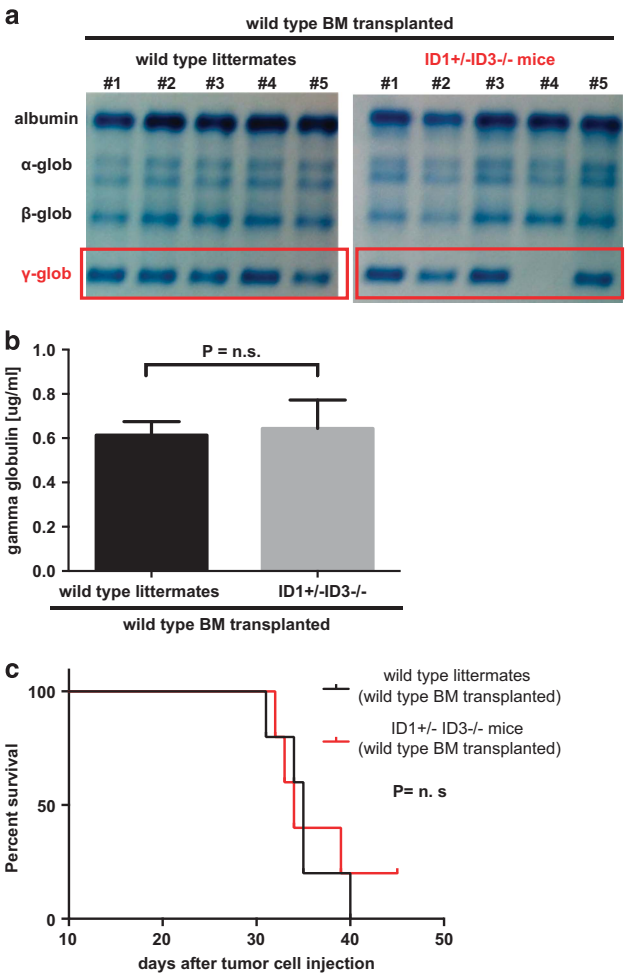

Figure 6. Wild-type BM transplantation restores Vk*MYC tumor growth in ID1+/− ID3−/− transgenic mice. (**a**) SPEP agarose gel results of wild-type BM-transplanted wild-type littermates ($n = 5$), and wild-type BM-transplanted ID1+/− ID3−/− mice ($n = 5$) 3 weeks after injection of Vk*MYC transplantable cell line (4×10^6 total spleen cells) showing the presence of an M-protein in the gamma region of the SPEP pattern of similar intensity in the group of wild-type BM-transplanted wild-type littermates and wild-type BM-transplanted ID1+/− ID3−/− mice. (**b**) Serum gamma globulin concentration estimated by QuickScan 2000 software in the same groups of mice and at the same time point. Values expressed as mean+s.e.m. *P* indicated *P*-value. (**c**) Kaplan–Meier survival curves of wild-type littermates ($n = 5$) and ID1+/− ID3−/− mice ($n = 5$) injected with transplantable Vk*MYC cells (4×10^6 total spleen cells). *P* indicated *P*-value by log-rank test.

Figure 7. Smoldering-like MM1.S-RFP-luc+ cells are more dependent on vasculature for their proliferation. (**a**) Kaplan–Meier survival curves of SCID-bg ($n = 5$) mice injected with either MM1.S-GFP-luc+ cells (5×10^6) or MM1.S-RFP-luc+ isogenic cells (5×10^6); survival of mice injected with smoldering-like MM1.S-RFP-luc+ cells was approximately three times longer than that of MM1.S-GFP-luc+ cell injected mice. (**b**, **c**) Luciferase proliferation assay of MM1.S-GFP-luc+ and MM1.S-RFP-luc+ cells after 24 of co-culture with HUVECs (**b**) or primary MM patients' ECFCs (**c**); compared with monoculture. Both HUVEC and ECFC co-cultures were able to significantly increase proliferation of the smoldering-like MM1.S-RFP-luc+ cells but not that of aggressive MM1.S-GFP-luc+ cells. (**d**) Gene set enrichment analysis (GSEA) plots (Enrichment Score) for several angiogenesis-related genesets analyzed in MM1.S-GFP-luc+ cells co-cultured with ECs compared with MM1.S-GFP-luc+ cells alone (upper panels), in MM1.S-RFP-luc+ cells co-cultured with ECs compared with MM1.S-RFP-luc+ cells alone (middle panels), and in MM1.S-GFP-luc+ cells alone compared with MM1.S-RFP-luc+ cells alone (lower panels). Angiogenesis-related genesets were enriched when MM1.S cells (both MM1.S-GFP-luc+ and MM1.S-RFP-luc+ cells) were co-cultured with ECs compared with when they were cultured alone. FDR indicates false discovery rate always and *P* indicates *P*-values and are shown per each geneset analyzed. (**e**) GSEA plots (Enrichment Score) for the cell-cycle KEGG, Reactome and Biocarta genesets analyzed in MM1.S-RFP-luc+ cells compared with MM1.S-RFP-luc+ cells alone (upper panels); in MM1.S-GFP-luc+ cells co-cultured with ECs compared to MM1.S-GFP-luc+ cells alone (middle panels); and MM1.S-GFP-luc+ cells alone compared with MM1.S-RFP-luc+ cells alone. The green curves show the enrichment score and reflect the degree to which each gene (black vertical lines) is represented at the top or bottom of the ranked gene list. Cell cycle-related genesets were enriched only when MM1.S-RFP-luc+ cells co-cultured with ECs were compared with MM1.S-RFP-luc+ cells alone. FDR indicates false discovery rate always and *P* indicates *P*-values and are shown per each geneset analyzed.

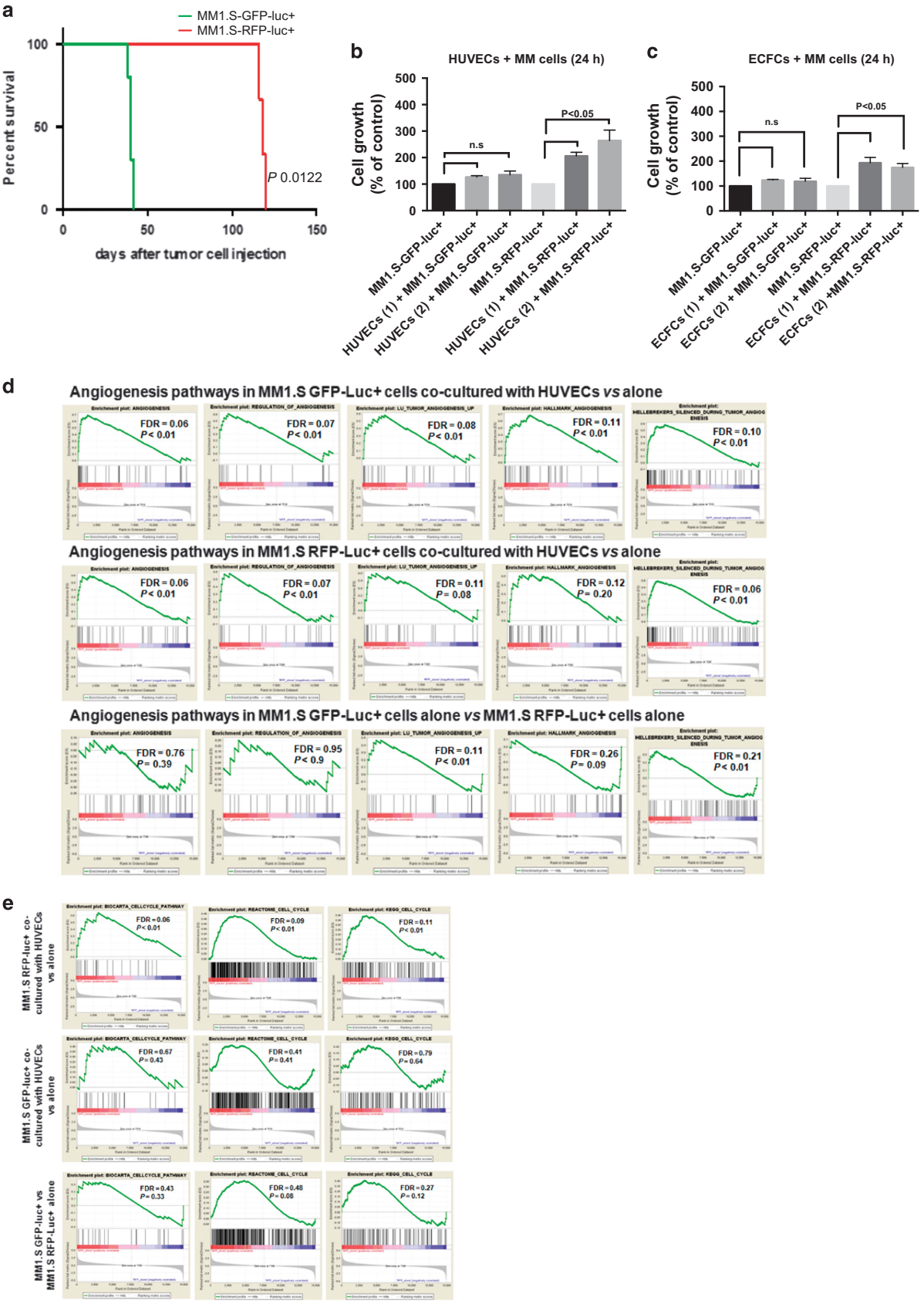

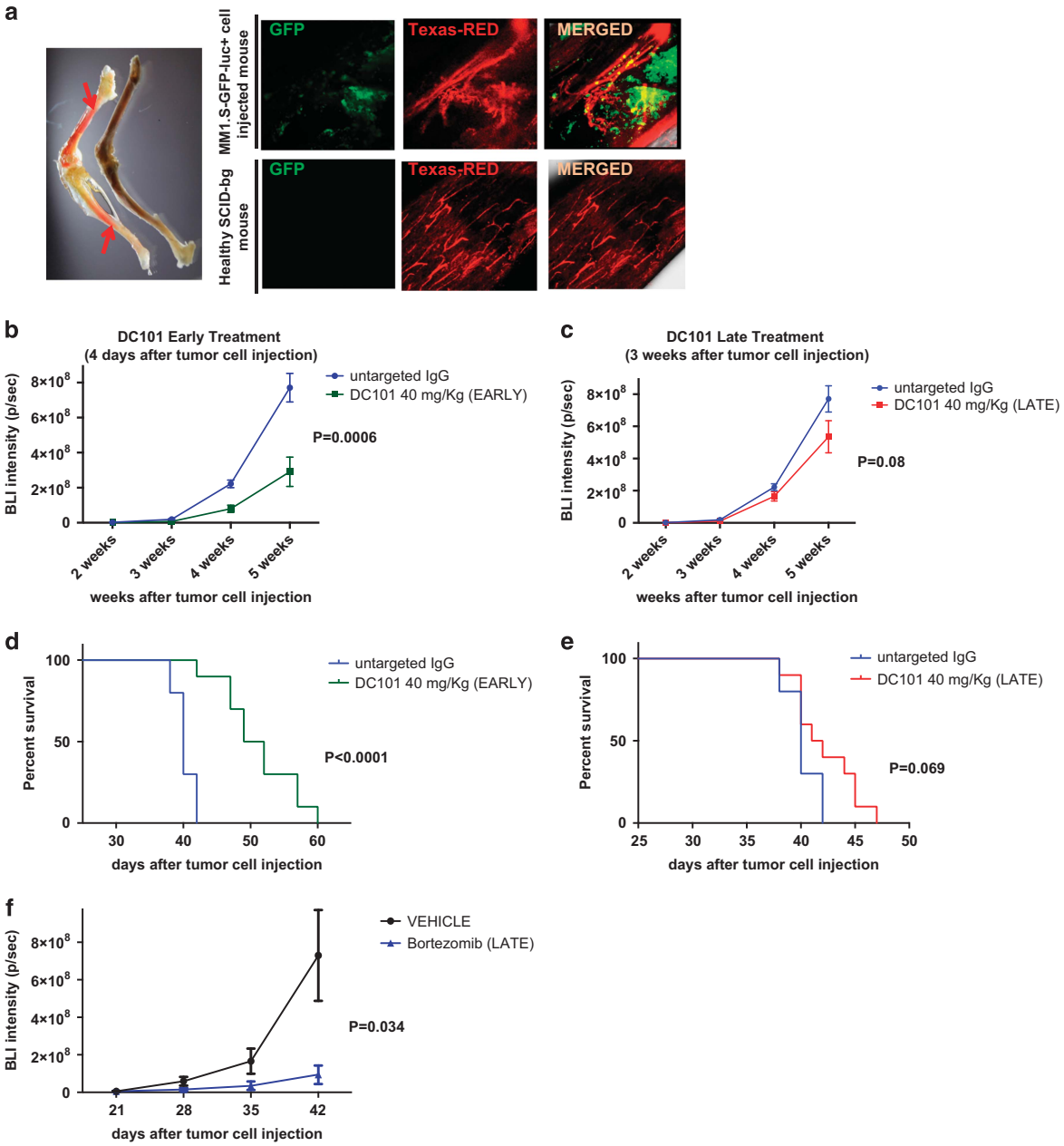

Figure 8. Early treatment with DC101 anti-VEGFR2 Ab delays MM tumor progression. (**a**) SCID-bg mice injected with MM1.S cells ($n=3$, 5×10^6 cells) and healthy SCID-bg mice ($n=2$) were injected with texas-red lectin i.v. then the mice were killed; femurs were clear, unobstructed brain/body imaging cocktails and computational analysis-treated (a representative femur is shown in the left panel indicated by arrows) to make them transparent; *ex vivo* BM confocal was performed directly in these femurs (right panels), showing the presence of GFP+ cells together with functional neovessels vascularizing clusters of MM GFP+ cells (right upper panels, ×30 magnification). The BM vasculature pattern is disorganized compared with that of a healthy mouse (right panels), suggesting pathological BM neovessel formation in tumor-bearing mice. (**b**) Tumor growth curves evaluated by BLI imaging in MM1.S-GFP-luc+ cell i.v. injected SCID-bg mice (5×10^6 cells) treated with untargeted IgG (40 mg/kg body weight (BW) at 3-day intervals, $n=10$) or DC101 anti-VEGFR2 Ab (40 mg/kg BW at 3-day intervals $n=10$) started 4 days after tumor cell injection (early treatment). (**c**) Comparison of tumor growth evaluated by BLI imaging in the same untargeted IgG-treated mice and the late DC101 anti-VEGFR2 Ab (40 mg/kg BW at 3-day intervals started 3 weeks after tumor cell injection, $n=10$) treated mice. Values expressed as mean ± s.e.m. *P* indicates *P*-value. (**d**) Kaplan–Meier survival curves of untargeted IgG (blue line) and early DC101 anti-VEGFR2 Ab (green line) treated mice. (**e**) Kaplan–Meier survival curves of the untargeted IgG (blue line) or late DC101 anti-VEGFR2 Ab (red line) treated mice. (**f**) Tumor growth evaluated by BLI imaging of MM1.S-GFP-luc+ cell i.v. injected SCID-bg mice (5×10^6 cells) treated with PBS (200 µl i.p., $n=7$) or bortezomib (0.5 mg/kg, twice/week; i.p., $n=7$) started 3 weeks after tumor cell injection (same as DC101 late schedule) showing significant anti-tumor activity. Values expressed as mean ± s.e.m. *P* indicates *P*-value.

we transplanted wild-type BM (from syngenic wild-type littermates) into ID1+/− ID3−/− mice and wild-type littermates, injected them with Vk12598 tumor cells, and examined the rate of progression of Vk12598 tumors in these mice. Tumor growth was restored in the ID1+/− ID3−/− mice transplanted with wild-type BM, as evidenced by similar M-spike levels in these mice and wild-type controls (Figures 6a and b). Moreover, survival of mice in the two groups was not significantly different (Figure 6c), indicating

that, indeed, the lack of EPCs in ID1+/− ID3−/− affects the growth of MM and restoring wild-type BM recovers tumor progression.

Smoldering-like MM cells are more dependent on vasculature for their proliferative activity

We developed two isogenic sub-clones of MM1.S, a GFP-luc+ MM1.S clone that presents with a more aggressive (active MM-like) *in vivo* tumor growth; and an RFP-luc+ MM1.S clone, characterized by a more indolent behavior (sMM-like). Mice injected with MM1.S-RFP-Luc+ cells presented with an overall survival three times longer compared with those injected with equal number of the isogenic MM1.S-GFP-luc+ cells (*P* 0.0122; Figure 7a).

We next tested whether a slower growing MM clone (as in sMM; MM1.S-RFP-luc+) is more dependent on the external stimuli provided by surrounding ECs and EPCs; while a more aggressive clone (as in active MM; MM1.S-GFP-luc+) is less dependent on external microenvironmental support. By comparing the proliferation of these isogenic sub-clones in co-culture with HUVECs or MM patient-derived ECFCs, we found a statistically significant proliferative increase in the smoldering-like clone (MM1.S-RFP-luc+) when cultured in the presence of either HUVECs or primary MM patient-derived ECFCs, for 24 h. In contrast, this HUVEC- or ECFC-induced growth advantage was less evident when active MM-like clones (MM1.S-GFP-luc+) were tested (Figures 7b and c). Similar results were observed at 48 and 72 h (Supplementary Figure 6A–D).

To further define the mechanism of this dependency of the tumor cells on endothelial cells, we performed RNA sequencing of flow-sorted MM1.S-GFP-luc+ and MM1.S-RFP-luc+ cells alone or co-cultured with ECs (Supplementary Figure 7A–C). Gene set enrichment analysis showed a consistent enrichment of angiogenesis-related genes in both MM1.S-GFP-luc+ and MM1.S-RFP-luc+ cells when co-cultured with ECs as compared with MM1.S-GFP-luc+ or MM1.S-RFP-luc+ cells cultured alone. These findings suggest that the interaction of either active MM-like or sMM-like cells with ECs activates pro-angiogenic programs in MM cells (Figure 7d, upper and middle panels). MM1.S-GFP-luc+ cultured alone as compared with MM1.S-RFP-luc+ cells cultured alone showed a significant enrichment of pro-angiogenic-related pathways, thus indicating that the active MM-like MM cells (MM1.S-GFP-luc+) present with a constitutive enrichment of pro-angiogenic relevant genes, compared with the smoldering-like MM1.S-RFP-luc+ (Figure 7d, lower panels). Interestingly, when we performed gene enrichment of genesets related to cell cycle and proliferation, we found that these were significantly enriched only when we compared MM1.S-RFP-luc+ cells co-cultured with ECs to MM1.S-RFP-luc+ cells alone (Figure 7e, upper panels). There was no significant enrichment when comparing MM1.S-GFP-luc+ cells co-cultured with ECs to MM1.S-GFP-luc+ cells alone (Figure 7e, middle and lower panels), indicating that ECs promote proliferation and cell-cycle regulation in the smoldering-like MM cells but not in the active-like MM1.S-GFP-luc+ cells (Supplementary Tables 1 and 2). To validate the RNA-sequencing data, we studied cell cycle and apoptosis of MM1.S-GFP-luc+ and MM1.S-RFP-luc+ cells co-cultured with ECs by flow cytometry. As shown in Supplementary Figure 8A and B, there was a significant induction of cell-cycle progression and reduction of apoptosis in MM1.S-RFP-luc+ cells that were co-cultured with ECs but not in MM1.S-GFP-luc+ cells. Therefore, targeting ECs at early stages of MM disease development may better exploit therapeutic potentialities of vessel targeting drugs in MM.

Targeting EPCs to prevent tumor progression in MM

The anti-murine VEGFR2 antibody (Ab) DC101 prevents mobilization and recruitment of BM-derived EPCs,[27,35] and was used to examine whether targeting EPCs can prevent tumor progression in MM. To avoid a possible confound by direct anti-tumor activity of the murine Ab in assessing the effects of EPC targeting in MM, we used a human MM1.S-GFP-luc+ orthotopic xenograft model. We first explored whether MM progression in this model is accompanied by BM neovessel formation by injecting (i.v.) MM1.S tumor-bearing mice and healthy control mice with texas-red conjugated tomato-lectin before killing, in order to stain perfused functional vessels. Femurs were harvested and treated with clear, unobstructed brain/body imaging cocktails and computational analysis,[20] in order to make them transparent (Figure 8a) and permit *ex vivo* intra-BM confocal imaging. Figure 8a shows the presence of GFP+ tumor cells in the BM, surrounded by small, perfused neovessels that enter the tumor clusters, and a change in the physiological BM vessel architecture observed in healthy mice. These observations confirmed that BM neovessels form in the MM1.S xenograft model.

Given that we observed that EPCs increase in the circulation in the early smoldering stages of MM and that at this stage MM cells are more dependent on BM ECs for their proliferation, we hypothesized that early treatment with DC101-Ab will prevent early EPC mobilization and tumor progression, while late treatment with the antibody, after significant tumor establishment, will not significantly affect tumor progression. Indeed, early administration of the DC101-Ab (started 4 days after injection of MM1.S-GFP-luc+ cells) led to a significant delay in tumor progression compared with mice treated with IgG control, and compared with mice receiving late treatment (started 3 weeks after injection of MM1.S-GFP-luc+ cells) (Figures 8b and c). Importantly, mice treated with the early schedule of DC101-Ab treatment showed a significant survival improvement (Figure 8d), while the late treated mice (Figure 8e) resulted in survival similar to that of mice treated with IgG control. No signs of toxicity or body weight loss was observed in the DC101-Ab-treated animals. Of note, bortezomib treatment started as late schedule of DC101-Ab treatment still exerted significant anti-MM activity in the MM1.S-GFP-luc+ model (Figure 8g). These results suggest that EPC targeting drugs may be effective for the treatment of early-stage myeloma (sMM) but not in late stages of overt MM.

DISCUSSION

EPCs promote tumor progression in solid cancers in preclinical models and in patients,[37,38] yet their role in regulating progression in hematological malignancies that reside within the BM has not been well defined. Here, we show that EPCs are mobilized to the PB of patients at early stages of sMM; and recruited from the BM to areas of disease colonization in other BM niches. We demonstrate that EPCs are critical for tumor progression in mouse models of MM, and that regulation of EPC trafficking using ID1+/− ID3−/− transgenic mice, or with use of the monoclonal DC101 antibody therapy, leads to a significant reduction of tumor progression. Notably, transplantation of wild-type BM in ID1+/− ID3−/− restored the growth of MM cells in the BM, indicating that indeed EPCs derived from the BM are critical for progression of cancers that reside in the BM, such as MM.

We also demonstrate that angiogenic dependency occurs early, during stages of sMM: in patient samples and mouse models, mobilization of EPCs occurs at early stages of disease progression, documenting that EPC circulation precedes MM progression. Moreover, we were able to successfully generate two MM1.S sub-clones with different *in vivo* growth rate, and showed that indeed EC interaction promotes a strong proliferative effect in smoldering-like MM clone but not in the more aggressive active-like MM clone. These were further confirmed using RNA-sequencing and flow-cytometry studies, demonstrating that ECs can enhance proliferation, cell cycle and apoptosis regulation only in MM clones that are

smoldering-like and have non-cell autonomous dependency on EC. Overall, the data presented here show that MM cells induce BM mobilization of EPCs, and stimulate their proliferation in both BM and PB. EPCs are then recruited into MM-enriched BM niches, where they transform into mature ECs thus contributing to the increase in neovessel formation observed in smoldering and active MM patients. Mature ECs then interact with MM cells promoting their proliferation and survival.

We hypothesized that early therapeutic intervention to prevent EPC circulation will prevent progression in MM, while delayed intervention after significant tumor colonization and independence of BM microenvironment stimuli will not have a beneficial effect. Our observations with the use of DC101 confirm this hypothesis and delineate a potential therapeutic intervention for patients who are in early stages of disease progression, such as in sMM.

Many agents, including immunomodulators[39,40] and proteasome inhibitors,[41,42] have been surveyed for their anti-angiogenic activity in MM. However, specific anti-angiogenic agents have not shown promising activity in the treatment of MM or other hematological malignancies,[5] despite their routine use in the treatment of solid tumors.[4] Here, we demonstrate that the apparent ineffectiveness of these agents may be a function of the time at which they are administered. Thus, although angiogenesis and MVD are high in active myeloma, the dependency of the tumor cells on EPCs and vasculogenesis may actually precede this step. This novel concept of manipulating vasculogenesis at an *early* stage of disease should be examined in future clinical trials in patients with sMM. Of note, the anti-human version of the DC101, namely ramucirumab, has been clinically developed and it is FDA approved for advanced gastro-esophageal adenocarcinoma and metastatic non-small-cell lung carcinoma. This preclinical study supports the investigation of this specific drug in future clinical trials in sMM patients.

In summary, our findings show that vasculogenesis is of critical importance in promoting early vessel formation, and is permissive for MM progression at early, but not later, stages of the disease; neovessel targeting agents should be used at early time points in these cancers where early intervention during angiogenic dependency is crucial for their activity.

CONFLICT OF INTEREST

The authors declare no conflict of interest.

ACKNOWLEDGEMENTS

We wish to thank the Animal Research Facility (ARF) team of the Dana Farber Cancer Institute for the valuable technical support. We thank Dr Benezra R (Memorial Sloan–Kettering Institute, NY, USA) for providing us the ID1/ID3 transgenic mice. We thank Sonal Jhaveri (PGSAO, Dana Farber Cancer Institute) for editing the manuscript. We thank Eli Lilly & Co. for providing the DC101 antibody. This work was supported by NIH R01 CA181683-01A1 and the Leukemia and Lymphoma Society. This work was supported by Associazione Italiana per la Ricerca sul Cancro, AIRC 5 × 1000 Molecular Clinical Oncology Special Program, Milan, IT (grant no. 9965 to M Bellone and A Vacca). Arianna Calcinotto was awarded a fellowship from AIRC/FIRC and conducted this study in partial fulfillment of her PhD at San Raffaele University.

AUTHOR CONTRIBUTIONS

MM and IMG contributed to conception and design. YM, YK, BP, LP, YA, AC, CU, IS, AS, SG, JS, MRR and SM contributed to acquisition of data. MM, YM, YK, AMR and IMG contributed to analysis and interpretation of data. MM, MB, MC, FP, PLB, AMR and IMG contributed to writing, review and/or revision of the manuscript.

REFERENCES

1 Moehler TM, Ho AD, Goldschmidt H, Barlogie B. Angiogenesis in hematologic malignancies. *Crit Rev Oncol Hematol* 2003; **45**: 227–244.
2 Dong X, Han ZC, Yang R. Angiogenesis and antiangiogenic therapy in hematologic malignancies. *Crit Rev Oncol Hematol* 2007; **62**: 105–118.
3 Eleutherakis-Papaiakovou V, Karali M, Kokkonouzis I, Tiliakos I, Dimopoulos MA. Bone marrow angiogenesis and progression in multiple myeloma: clinical significance and therapeutic approach. *Leuk Lymphoma* 2003; **44**: 937–948.
4 Carmeliet P, Jain RK. Molecular mechanisms and clinical applications of angiogenesis. *Nature* 2011; **473**: 298–307.
5 Li WW, Hutnik M, Gehr G. Antiangiogenesis in haematological malignancies. *Br J Haematol* 2008; **143**: 622–631.
6 Somlo G, Lashkari A, Bellamy W, Zimmerman TM, Tuscano JM, O'Donnell MR *et al.* Phase II randomized trial of bevacizumab versus bevacizumab and thalidomide for relapsed/refractory multiple myeloma: a California Cancer Consortium trial. *Br J Haematol* 2011; **154**: 533–535.
7 Ria R, Reale A, De Luisi A, Ferrucci A, Moschetta M, Vacca A. Bone marrow angiogenesis and progression in multiple myeloma. *Am J Bood Res* 2011; **1**: 76–89.
8 Ziyad S, Iruela-Arispe ML. Molecular mechanisms of tumor angiogenesis. *Genes Cancer* 2011; **2**: 1085–1096.
9 Moschetta M, Mishima Y, Sahin I, Manier S, Glavey S, Vacca *et al.* Role of endothelial progenitor cells in cancer progression. *Biochim Biophys Acta* 2014; **1846**: 26–39.
10 Bhutani M, Turkbey B, Tan E, Kemp TJ, Pinto LA, Berg AR *et al.* Bone marrow angiogenesis in myeloma and its precursor disease: a prospective clinical trial. *Leukemia* 2014; **28**: 413–416.
11 Kyle RA, Rajkumar SV. Criteria for diagnosis, staging, risk stratification and response assessment of multiple myeloma. *Leukemia* 2009; **23**: 3–9.
12 Hill JM, Zalos G, Halcox JP, Schenke WH, Waclawiw MA, Quyyumi AA *et al.* Circulating endothelial progenitor cells, vascular function, and cardiovascular risk. *N Engl J Med* 2003; **348**: 593–600.
13 Martin-Ramirez J, Hofman M, van den Biggelaar M, Hebbel RP, Voorberg J. Establishment of outgrowth endothelial cells from peripheral blood. *Nat Protoc* 2012; **7**: 1709–1715.
14 Azab AK, Sahin I, Azab F, Moschetta M, Mishima Y, Burwick N *et al.* CXCR7-dependent angiogenic mononuclear cells trafficking regulates tumor progression in multiple myeloma. *Blood* 2014; **124**: 1905–1914.
15 Roccaro AM, Sacco A, Maiso P, Azab AK, Tai YT, Reagan M *et al.* BM mesenchymal stromal cell-derived exosomes facilitate multiple myeloma progression. *J Clin Invest* 2013; **123**: 1542–1555.
16 Chesi M, Matthews GM, Garbitt VM, Palmer SE, Shortt J, Lefebure M *et al.* Drug response in a genetically engineered mouse model of multiple myeloma is predictive of clinical efficacy. *Blood* 2012; **120**: 376–385.
17 Roccaro AM, Sacco A, Jimenez C, Maiso P, Moschetta M, Mishima Y *et al.* C1013G/CXCR4 acts as a driver mutation of tumor progression and modulator of drug resistance in lymphoplasmacytic lymphoma. *Blood* 2014; **123**: 4120–4131.
18 Bendall SC, Simonds EF, Qiu P, Amir el AD, Krutzik PO, Finck R *et al.* Single-cell mass cytometry of differential immune and drug responses across a human hematopoietic continuum. *Science* 2011; **332**: 687–696.
19 Bodenmiller B, Zunder ER, Finck R, Chen TJ, Savig ES, Bruggner RV *et al.* Multiplexed mass cytometry profiling of cellular states perturbed by small-molecule regulators. *Nat Biotechnol* 2012; **30**: 858–867.
20 Susaki EA, Tainaka K, Perrin D, Kishino F, Tawara T, Watanabe TM *et al.* Whole-brain imaging with single-cell resolution using chemical cocktails and computational analysis. *Cell* 2014; **157**: 726–739.
21 Werner N, Kosiol S, Schiegl T, Ahlers P, Walenta K, Link *et al.* Circulating endothelial progenitor cells and cardiovascular outcomes. *N Engl J Med* 2005; **353**: 999–1007.
22 Lin Y, Weisdorf DJ, Solovey A, Hebbel RP. Origins of circulating endothelial cells and endothelial outgrowth from blood. *J Clin Invest* 2000; **105**: 71–77.
23 Yoder MC, Mead LE, Prater D, Krier TR, Mroueh KN, Li F *et al.* Redefining endothelial progenitor cells via clonal analysis and hematopoietic stem/progenitor cell principals. *Blood* 2007; **109**: 1801–1809.
24 Yoder MC, Ingram DA. The definition of EPCs and other bone marrow cells contributing to neoangiogenesis and tumor growth: is there common ground for understanding the roles of numerous marrow-derived cells in the neoangiogenic process? *Biochim Biophys Acta* 2009; **1796**: 50–54.
25 Zhang H, Vakil V, Braunstein M, Smith EL, Maroney J, Chen L *et al.* Circulating endothelial progenitor cells in multiple myeloma: implications and significance. *Blood* 2005; **105**: 3286–3294.
26 Bhaskar A, Gupta R, Kumar L, Sharma A, Sharma MC, Kalaivani M *et al.* Circulating endothelial progenitor cells as potential prognostic biomarker in multiple myeloma. *Leuk Lymphoma* 2012; **53**: 635–640.
27 Taylor M, Billiot F, Marty V, Rouffiac V, Cohen P, Tournay E *et al.* Reversing resistance to vascular-disrupting agents by blocking late mobilization of circulating endothelial progenitor cells. *Cancer Discov* 2012; **2**: 434–449.

28 Chakroborty D, Chowdhury UR, Sarkar C, Baral R, Dasgupta PS, Basu S. Dopamine regulates endothelial progenitor cell mobilization from mouse bone marrow in tumor vascularization. *J Clin Invest* 2008; **118**: 1380–1389.
29 Chesi M, Robbiani DF, Sebag M, Chng WJ, Affer M, Tiedemann R *et al.* AID-dependent activation of a MYC transgene induces multiple myeloma in a conditional mouse model of post-germinal center malignancies. *Cancer Cell* 2008; **13**: 167–180.
30 Calcinotto A, Ponzoni M, Ria R, Grioni M, Cattaneo E, Villa I *et al.* Modifications of the mouse bone marrow microenvironment favor angiogenesis and correlate with disease progression from asymptomatic to symptomatic multiple myeloma. *Oncoimmunology* 2015; **4**: e1008850.
31 Mitsiades CS, Anderson KC, Carrasco DR. Mouse models of human myeloma. *Hematol Oncol Clin North Am* 2007; **21**: 1051–1069, viii.
32 Vacca A, Ribatti D, Roncali L, Ranieri G, Serio G, Silvestris F *et al.* Bone marrow angiogenesis and progression in multiple myeloma. *Br J Haematol* 1994; **87**: 503–508.
33 Rajkumar SV, Leong T, Roche PC, Fonseca R, Dispenzieri A, Lacy MQ *et al.* Prognostic value of bone marrow angiogenesis in multiple myeloma. *Clin Cancer Res* 2000; **6**: 3111–3116.
34 Lyden D, Young AZ, Zagzag D, Yan W, Gerald W, O'Reilly R *et al.* Id1 and Id3 are required for neurogenesis, angiogenesis and vascularization of tumour xenografts. *Nature* 1999; **401**: 670–677.
35 Lyden D, Hattori K, Dias S, Costa C, Blaikie P, Butros L *et al.* Impaired recruitment of bone-marrow-derived endothelial and hematopoietic precursor cells blocks tumor angiogenesis and growth. *Nat Med* 2001; **7**: 1194–1201.
36 Ciarrocchi A, Jankovic V, Shaked Y, Nolan DJ, Mittal V, Kerbel RS *et al.* Id1 restrains p21 expression to control endothelial progenitor cell formation. *PLoS One* 2007; **2**: e1338.
37 Gao D, Nolan D, McDonnell K, Vahdat L, Benezra R, Altorki N *et al.* Bone marrow-derived endothelial progenitor cells contribute to the angiogenic switch in tumor growth and metastatic progression. *Biochim Biophys Acta* 2009; **1796**: 33–40.
38 Roodhart JM, Langenberg MH, Daenen LG, Voest EE. Translating preclinical findings of (endothelial) progenitor cell mobilization into the clinic; from bedside to bench and back. *Biochim Biophys Acta* 2009; **1796**: 41–49.
39 De Luisi A, Ferrucci A, Coluccia AM, Ria R, Moschetta M, de Luca E *et al.* Lenalidomide restrains motility and overangiogenic potential of bone marrow endothelial cells in patients with active multiple myeloma. *Clin Cancer Res* 2011; **17**: 1935–1946.
40 Vacca A, Scavelli C, Montefusco V, Di Pietro G, Neri A, Mattioli M *et al.* Thalidomide downregulates angiogenic genes in bone marrow endothelial cells of patients with active multiple myeloma. *J Clin Oncol* 2005; **23**: 5334–5346.
41 Roccaro AM, Hideshima T, Raje N, Kumar S, Ishitsuka K, Yasui H *et al.* Bortezomib mediates antiangiogenesis in multiple myeloma via direct and indirect effects on endothelial cells. *Cancer Res* 2006; **66**: 184–191.
42 Moschetta M, Di Pietro G, Ria R, Gnoni A, Mangialardi G, Guarini *et al.* Bortezomib and zoledronic acid on angiogenic and vasculogenic activities of bone marrow macrophages in patients with multiple myeloma. *Eur J Cancer* 2010; **46**: 420–429.

Supplementary Information accompanies this paper on the Leukemia website (http://www.nature.com/leu)